
A COMPARISON OF PRE-TRAINED VISION-AND-LANGUAGE MODELS FOR MULTIMODAL REPRESENTATION LEARNING ACROSS MEDICAL IMAGES AND REPORTS

Yikuan Li

Feinberg School of Medicine
Northwestern University
Chicago, IL 60611
yikuanli2018@u.northwestern.edu

Hanyin Wang

Feinberg School of Medicine
Northwestern University
Chicago, IL 60611
hanyinwang2022@u.northwestern.edu

Yuan Luo*

Feinberg School of Medicine
Northwestern University
Chicago, IL 60611
yuan.luo@northwestern.edu

ABSTRACT

Joint image-text embedding extracted from medical images and associated contextual reports is the bedrock for most biomedical vision-and-language (V+L) tasks, including medical visual question answering, clinical image-text retrieval, clinical report auto-generation. In this study, we adopt four pre-trained V+L models: LXMERT, VisualBERT, UNIER and PixelBERT to learn multimodal representation from MIMIC-CXR radiographs and associated reports. The extrinsic evaluation on OpenI dataset shows that in comparison to the pioneering CNN-RNN model, the joint embedding learned by pre-trained V+L models demonstrate performance improvement in the thoracic findings classification task. We conduct an ablation study to analyze the contribution of certain model components and validate the advantage of joint embedding over text-only embedding. We also visualize attention maps to illustrate the attention mechanism of V+L models.

1 Introduction

There has been a long history of learning visual and semantic information to solve vision and language tasks. Various pioneering approaches [1, 2, 3, 4, 5] have been proposed to boost the performance of visual question answering (VQA) [6], image captioning, image-text matching, visual reasoning [7] and textual grounding, respectively. These models learned image representations from powerful backbone convolutional neural networks (CNN), text representations from recurrent neural networks (RNN), and a fusion modality to achieve joint image-text embedding. For simplicity, these genres of models are often referred to as CNN+RNN models. Most of these models were designed for specific vision-and-language tasks and therefore had relatively poor generalizability. Recently, inspired by the success of large-scale pre-trained language models, such as BERT [8], XLNET [9], more researchers focus on generating image-text joint embedding from pre-training Transformer-based [10] model on V+L datasets. The joint embedding is then fine-tuned to various V+L tasks and achieves state-of-the-art results. The main difference between these models lies in pre-training strategies and cross-modality architecture. To be specific, UNITER [11] and VisualBert [12] applied a single stream of Transformer to jointly learn image-text embedding. LXMERT [13] and ViLBERT [14] used two separated Transformer blocks on image and text input and a third fusion Transformer block for cross-modality. Masked language modeling,

*Corresponding author

Our implementation can be found at: <https://github.com/YIKUAN8/Transformers-VQA>

masked region modeling, image-text matching, word-region alignment, and other pre-training tasks are experimented in those models.

The joint image-text embedding are less discussed in the biomedical domain due to the shortage of large-scale annotated V+L datasets. TandemNet [15], which adopts a CNN+LSTM architecture, classifies pathological bladder cancer from images with the semantic clues in diagnostic reports. Lau et al. [16] introduce the first manually constructed VQA dataset in radiology, named VQA-RAD. In their study, the performances of 2 well-known CNN+LSTM architecture (MCB [17] and SAN [18]) are compared with human radiologists on the VQA-RAD dataset. For drug label identification tasks, the image-text embedding (DLI-IT) [19] derived from an VGG+BiLSTM architecture, greatly outperforms image-based or text-based identification methods. Yan et al. [20] won the first place in ImageCLEF 2019 VQA-Med [21] competition using the "VGG16+BERT+MFB" model. Unlike conventional architectures using RNN for text embedding, they encode the semantic questions using the last and penultimate hidden states of the BERT model.

Chest X-Ray datasets are widely used in V+L researches. The joint image-text embedding can be learned from easily accessible Chest X-ray images and free-text radiology reports. TieNet [22], an end-to-end CNN+RNN architecture, is developed to learn a blend of distinctive image and text representations from the ChestXray14 [23] dataset and are further used for thoracic findings classification and automatic X-ray report generation. Zhang et al. [24] achieve better interpretation for OpenI [25] Chest X-Ray dataset by using dual attention mechanisms to distill visual features with semantic features. Hsu et al. [26] explore supervised and unsupervised methods to learn joint image-text embedding from MIMIC-CXR [27] dataset. The joint representations are further examined by a document retrieval task.

We observe that there is a significant gap between the models for joint embedding generation. Transformer-based pre-trained models are widely used in the general domain while in the biomedical domain, CNN-RNN based architectures are still predominating. Our contributions are three-fold: (1) We compare 4 pre-trained Transformer-based V+L models of learning joint image-text embedding from chest radiographs and associated reports; (2) We conduct extrinsic evaluation to compare these V+L models with a pioneering CNN-RNN model (TieNet); (3) We explore the advantage of joint embedding over text-only embedding, pre-training over train-from-scratch and other model components by a detailed ablation study.

2 Methodology

In this section, we introduce how to fine-tune pre-trained V+L models for a multi-label thoracic findings classifier from Chest X-ray images and associated reports. This experiment can be considered as a visual question answering (VQA) task. The workflow is illustrated in Fig. 1.

2.1 Data

2.1.1 MIMIC-CXR

MIMIC-CXR[27] is the largest publicly available Chest X-ray dataset that contains 377,110 radiographs and 227,827 free-text radiology associated reports. 13 thoracic findings (detailed in the ‘Finding’ column of Table 3) and ‘*No Finding*’ (absence of all 13 findings) are derived from radiology reports by using 2 auto-annotators: CheXpert [28] and NegBio [29]. Each label is categorized into one of four classes: *positive, negative, uncertain and missing*.

We pre-process the data as follows. First, as one radiology report can be associated with multiple radiographs, we only keep the first frontal view radiograph in chronological order. Those reports without any frontal view radiographs are discarded. Then, we re-categorize the labels of radiology reports from 4 classes: *positive, negative, uncertain and missing* to 2 classes: *positive and all others*. This step helps us keep our processed labels consistent with other public chest X-ray datasets (e.g. ChestXRay14, Open I). In total, we have 222,713 image-report pairs and each pair corresponds to 14 binary labels. The sample numbers and prevalence of each finding are shown in the #,% columns in Table 3.

2.2 Open I

OpenI[30] is another publicly available chest X-ray dataset collected by Indiana University. The dataset contains 3,996 radiology reports associated with 8,121 images. Unlike MIMIC-CXR, which is annotated by auto-annotators, OpenI dataset is labeled by medical professionals manually using Medical Subject Heading [31] (MeSH) indexing. We apply the same pre-processing steps as TieNet and yielded 3,684 image-report pairs. Each pair is assigned multiple MeSH terms by human-annotators. For comparison purposes, we only keep the findings that also present in MIMIC-CXR. The positive pair sample numbers and prevalence of selected findings are shown in the #,% columns in Table 2.

Figure 1: Overview of applying V+L models to learn joint image-text embedding from CXR images and associated reports for thoracic findings identification.

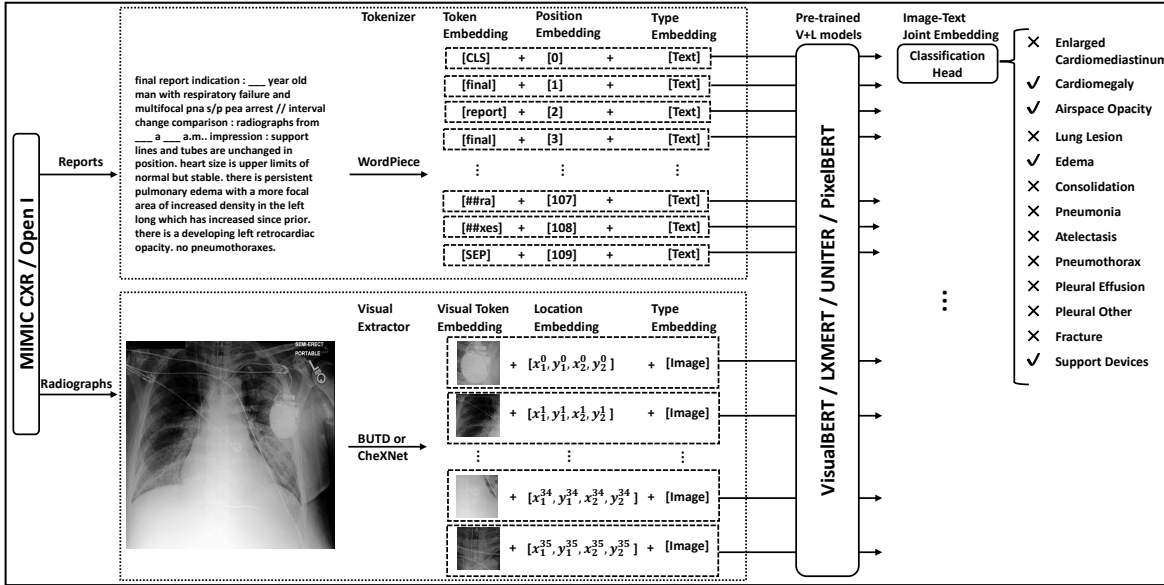


Table 1: A comparison across four pre-trained vision-and-language models and two language representation models.

Model	Pretraining Dataset	Pretraining Tasks*	Visual Encoder	Location Features	Model Architecture**	Transformer Streams	Baseline Performance***
UNITER [11]	COCO [32]+VG [33]+CC [34]+SBU [35]	MLM+MRM+ITM+WRA	BUTD [36]	[top, left, bottom, right, width, height, area] of ROIs	12 BertLayers	Single	72.70 (COCO)
LXMERT [13]	COCO+VG+VQA2.0 [6]+GQA [37]+VG-QA [38]	MLM+MRM+ITM+IQA	BUTD	[top, left, bottom, right] of ROIs	9 BertLayers for language, 5 BertLayers for vision, 5 CrossAttLayers for cross-modality	Double	72.40 (COCO)
VisualBERT [12]	COCO+VQA2.0	MLM+ITM+Task-specific Pretraining	BUTD	-	12 BertLayers	Single	70.80 (COCO)
PixelBERT [39]	COCO+VG	MLM+ITM	ResNeXt [40] (Trainable)	-	12 BertLayers	Single	74.45 (COCO)
BERT [41]	BookCorpus+English-Wiki [42]	MLM+NSP	-	-	12 BertLayers	Single	77.6 (MedNLI)
ClinicalBERT [43]	MIMIC-III [44]	MLM+NSP	-	-	12 BertLayers	Single	80.8 (MedNLI)

* MLM: Mask Language Modeling; MRM: Mask Region Modeling; ITM: Image-Text Matching; WRA: Word-Region Alignment; IQA: Image Question Answering; NSP: Next sentence prediction.

** BertLayer is a self-attention layer followed by a feed-forward layer; CrossAttLayer is a cross-attention layer followed by a feed-forward layer.

*** For V+L models, we report the accuracy performed on test-dev of COCO; For language representation models, we report the accuracy performed on MedNLI [45]

2.3 Models

We investigate 4 trending vision-and-language models: VisualBERT, UNITER, LXMERT, and PixelBERT. A detailed comparison of these models is outlined in Table 1. In summary, all 4 V+L models use the COCO [32] dataset as their pre-training material. Some other data sources, such as Visual Genome [33], VQA 2.0 [21] are added to enrich the training materials. Inspired by the masked language modeling (MLM) and next-sentence prediction of the BERT model, MLM conditioned on images and image-text matching (ITM) are adopted by all 4 V+L models. Only VisualBERT requires task-specific training to improve the performance on downstream tasks. Bottom-up top-down (BUTD) [36], adopted by VisualBERT, UNITER, and LXMERT, is the most common region-based visual encoder in V+L models. However, region-based visual encoders are designed for specific visual tasks and are limited by the given categories of the object detection tasks. PixelBERT creatively solves the limitation of region-based visual representation by proposing a CNN-based visual encoder. Note that the self-attention mechanism in the Transformer model is order-less, thus

Table 2: AUCs of identifying 7 thoracic findings from OpenI dataset using TieNet, 4 pre-trained vision-and-language models, and 2 language representation models.

Findings	Image+Report					Report			#	%
	TieNet-I+R	VisualBERT	LXMERT	UNITER	PixelBERT	TieNet-R	BERT	ClinicalBERT		
Cardiomegaly	0.962	0.977	0.980	0.978	0.970	0.944	0.976	0.969	315	8.55
Edema	0.995	0.982	0.995	0.989	0.995	0.984	0.987	0.976	40	1.09
Consolidation	0.989	0.996	0.993	0.998	0.975	0.969	0.978	0.982	28	0.76
Pneumonia	0.994	0.990	0.990	0.988	0.969	0.983	0.970	0.982	36	0.98
Atelectasis	0.972	0.992	0.989	0.982	0.959	0.981	0.927	0.947	293	7.95
Pneumothorax	0.960	0.988	0.958	0.983	0.982	0.960	0.930	0.973	22	0.60
Pleural Effusion	0.977	0.985	0.983	0.983	0.970	0.968	0.961	0.976	140	3.80
Average	0.978	0.987	0.984	0.986	0.974	0.970	0.961	0.972		
#w Average*	0.971	0.985	0.984	0.982	0.968	0.965	0.956	0.964		

*#w Averaged denotes the sample number weighted average of AUC.

UNITER and LXMERT employ one layer of location features in addition to the original visual features. LXMERT is the only model that has two transformer streams that learns visual and text embedding separately, and further incorporates them with cross-attention layers to achieve joint embedding.

Preliminary results show that TieNet-R, an attention-based LSTM model that only needs contextual input, also yielded a competitive result. This is in line with expectations since radiology reports are generated by experienced radiologists that contain richer and more interpretative information compared with images. Moreover, the finding labels are auto-annotated by CheXpert, a rule-based text classifier, on radiology reports. Therefore, it is natural that applying text-only embedding methods also achieves a good performance. To this end, BERT and ClinicalBERT [43], two pre-trained language representation models, are also involved in our study for the purpose of exploring the advantages of image-text joint embedding over text-only embedding. These two models have the same Transformer-based architecture as PixelBERT, VisualBERT, and UNITER. BERT obtained state-of-the-art results on 11 NLP tasks when released. ClinicalBERT, trained on MIMIC-III [44] dataset, enhances adaptability of BERT for the clinical domain and yields performance improvements on clinical NLP tasks.

2.4 Implementations

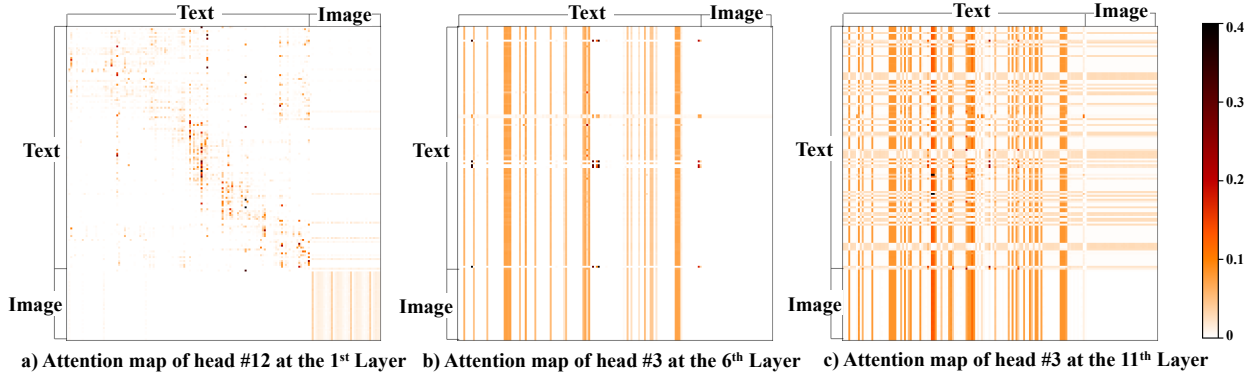
We first fine-tune the 4 V+L models to learn a joint image-text embedding (the last hidden-state of [CLS] token) from the training set of MIMIC-CXR. A classification head is added on top of the joint embedding to generate the probability estimates of 13 thoracic findings. We use the held-out testing set of MIMIC-CXR for internal evaluation and entire OpenI dataset for external evaluation. It should be noted that we do not follow the official splits of MIMIC-CXR. Instead, we perform stratified split and use 80% of the entire dataset as the training set, 10% as developing set for

Table 3: AUCs of identifying 13 thoracic findings from MIMIC-CXR dataset by fine-tuning 4 pre-trained vision-and-language models and 2 language representation models. Multiple configurations of each model are applied for ablation studies usage.

Findings	Image+Report										Report		#	%		
	Config*	LXMERT			VisualBERT			UNITER			PixelBERT				BERT	ClinicalBERT
		Default	FS	CB	Default	FS	CB	Default	FS	CB	Default	NT				
Enlarged-Cardiome-diastinum	0.974	0.971	0.971	0.981	0.856	0.977	0.979	0.866	0.962	0.870	0.724	0.747	0.966	7,025	3.15	
Cardiomegaly	0.987	0.988	0.988	0.991	0.968	0.990	0.989	0.974	0.981	0.965	0.814	0.954	0.979	43,931	19.73	
Air-space Opacity	0.988	0.988	0.988	0.991	0.977	0.989	0.989	0.981	0.984	0.971	0.922	0.972	0.978	50,238	22.56	
Lung Lesion	0.983	0.963	0.963	0.985	0.947	0.983	0.981	0.948	0.962	0.951	0.723	0.911	0.972	6,312	2.83	
Edema	0.988	0.989	0.988	0.991	0.975	0.990	0.990	0.978	0.985	0.958	0.790	0.956	0.979	26,309	11.81	
Consolidation	0.985	0.986	0.986	0.989	0.967	0.986	0.988	0.974	0.981	0.973	0.772	0.947	0.979	10,507	4.72	
Pneumonia	0.969	0.971	0.971	0.977	0.932	0.973	0.974	0.948	0.961	0.942	0.741	0.886	0.962	16,539	7.43	
Atelectasis	0.985	0.986	0.986	0.988	0.975	0.986	0.987	0.978	0.983	0.971	0.797	0.965	0.976	44,887	20.15	
Pneumothorax	0.990	0.985	0.985	0.992	0.975	0.991	0.991	0.981	0.985	0.942	0.827	0.942	0.979	10,432	4.68	
Pleural Effusion	0.990	0.991	0.991	0.993	0.982	0.992	0.992	0.984	0.988	0.972	0.945	0.967	0.981	52,890	23.75	
Pleural Others	0.983	0.969	0.969	0.981	0.946	0.973	0.973	0.956	0.963	0.930	0.735	0.815	0.964	1,949	0.88	
Fracture	0.979	0.976	0.976	0.976	0.960	0.975	0.977	0.956	0.961	0.941	0.602	0.873	0.958	4,425	1.99	
Support Devices	0.993	0.992	0.992	0.995	0.985	0.993	0.994	0.986	0.990	0.979	0.949	0.970	0.983	65,235	29.29	
Average	0.984	0.981	0.981	0.987	0.957	0.984	0.985	0.962	0.976	0.953	0.795	0.916	0.974			

* Configurations for ablation studies: Default: default configuration; FS: training from scratch without loading pre-trained model weights; CB: replacing the tokenizer, vocabulary and embedding layer with those of ClinicalBERT; NT: freezing weights of the visual backbone.

Figure 2: Visualization of the selected attention maps learned by the VisualBERT model.



hyper-parameter selection, and the rest 10% for held-out internal evaluation. TieNet [22], a pioneering joint embedding model used RNN-CNN architecture, is set as a baseline in our external evaluation. Areas Under Receiver Operating Curves (AUC) is computed based on the probability estimates and annotated labels to evaluate the model performance. We follow the evaluations in TieNet and report averaged AUC and sample number weighted average of AUC for comparison.

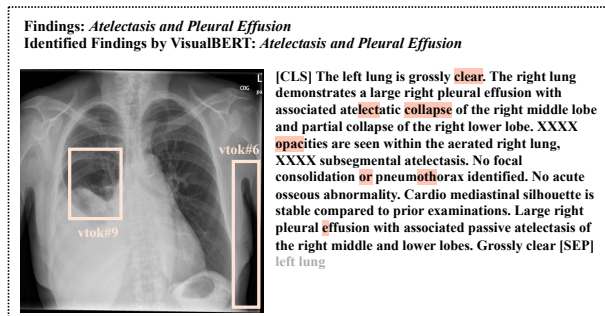
For detailed implementation, each text sequence is truncated or padded to 128 tokens in length. We apply a special edition of BUTD visual encoder for UNITER, LXMERT and VisualBERT, which consistently extracts 36 objects from a single image. As the pre-trained weights of PixelBERT are not open-sourced, we adopt CheXNet [46] as a substitute of the ResNeXt as the visual backbone and initialize the BertLayers with pre-trained BERT weights. The feature map (7x7x1024) of CheXNet is first flattened by spatial dimensions (49x1024) and then down-sampled to 36 1024-long visual features. We follow the same setting as [39] that trains the PixelBERT for 18 epochs. All other 3 V+L models as well as BERT and ClinicalBERT are fine-tuned for 6 epochs as the pre-trained weights can be loaded. SGD optimizer, with weight decay 5e-4 and learning rate 0.01 scheduled decay by 10 at the 12th and 16th epoch, is used to optimize the CheXNet backbone in PixelBERT. AdamW is used to optimize the Transformer block(s) in all models. Each model can be fit into 1 Tesla K40 GPU when using a batch size of 16. Our implementation can be found at: <https://github.com/YIKUAN8/Transformers-VQA>

3 Results

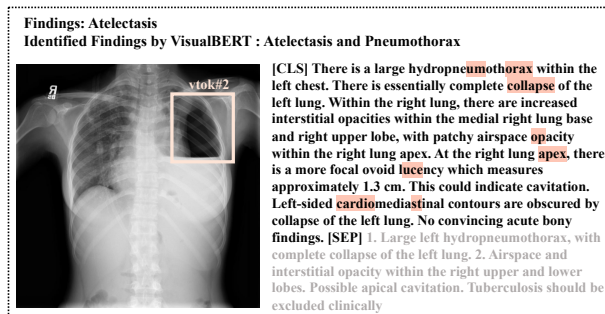
The model performance on OpenI dataset are shown in Table 2. All V+L models yield a high AUC of over 0.958 for all findings. VisualBERT, LXMERT and UNITER achieve higher averaged AUC (0.984+) and sample number weighted AUC (0.982+) than TieNet-I+R (0.978 and 0.971) in OpenI dataset. While PixelBERT, without any pre-training, performs slightly worse than TieNet-I+R. The supreme performance demonstrates all V+L models' great adaptability to biomedical domain. When digging into a particular finding, TieNet only outperforms V+L models in the classification of *edema* and *pneumonia*.

We use the held-out test split of MIMIC-CXR to make a more comprehensive comparison of 4 V+L models. The results are revealed in the *default* column of Table 3. VisualBERT yields the best averaged AUC of 0.987, followed by 0.985 using UNITER and 0.984 using LXMERT. PixelBERT only achieves a moderate AUC of 0.953 due to the absence of the pre-training. When comparing the performance on different findings, we surprisingly find that VisualBERT achieves the best results on 11 out of 13 findings. Although VisualBERT adopts the least pre-training tasks and the simplest model architecture, we believe the introduction of task-specific training for VQA contributes to this optimal performance. LXMERT outperforms others in *Pleural Others* and *Fracture*, which are the two least prevalent findings. We also notice that it is harder to identify *Enlarged Cardiomeastinum* compared with other abnormalities. We attribute this to the absence of lateral view X-ray images in our training set in that the cardiomeastinum contour is easier to recognize from a lateral view. Moreover, it is as expected that UNITER does not have a supreme performance in our study as we adopt the base version of UNITER. $UNITER_{larger}$ is much larger than $UNITER_{base}$ in both number of layers and trainable parameters. We believe that $UNITER_{larger}$ can achieve better results given its phenomenal performance in general domain.

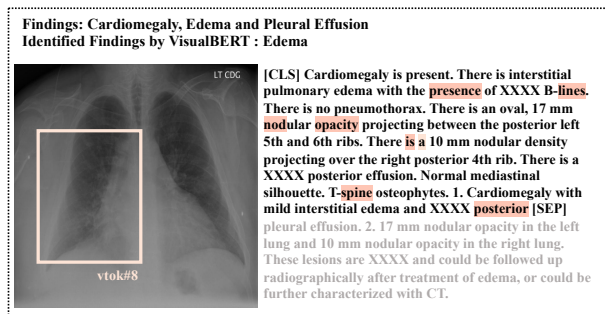
Figure 3: Results of three classification samples. Top 10 tokens with highest attention scores are highlighted in each sample. Words in grey are truncated during tokenization.



a) Top 10 tokens of a correctly identified case



b) Top 10 tokens of a false positive case



c) Top 10 tokens of a false negative case

Next, we compare the advantage of using image-text joint embedding over text-only embedding. When using joint embedding, TieNet only receives less than 1% performance improvement over the text-only embedding in the OpenI dataset. While, VisualBERT, LXMERT, and UNITER receives more than 2% improvement over BERT and 1% over ClinicalBERT, respectively. This larger performance improvement demonstrates that transformer-based models are better at image-text interaction compared with the CNN-RNN architecture. In the test split of MIMIC-CXR, the improvement of V+L models over BERT model is even larger (more than 6%).

Additionally, although VisualBERT, LXMERT, and UNITER have different model architectures, embedding, and pre-training strategies, they all yield comparable results in both internal held-out evaluation and external data resources. This is in line with expectation because these V+L models all have supreme performance and rank top 10 in the general domain (evaluated by coco test-dev). This also indicates that although BUTD is pre-trained in general domain from Visual Genome, it could also extract useful ROIs from biomedical images.

Table 4: Layer-level modality importance scores. A lower score indicates that [CLS] token spends less attention on the modality.

Layer#	1	2	3	4	5	6	7	8	9	10	11	12
Textual Modality Importance	0.828	0.993	0.941	0.824	0.844	0.908	0.724	0.733	0.812	0.864	0.922	0.673
Visual Modality Importance	0.170	0.007	0.055	0.103	0.147	0.082	0.254	0.206	0.172	0.134	0.075	0.324

4 Discussion

In this section, we first present ablation studies to analyze the contribution of certain model components. Then, we use visualization to illustrate the attention details. Finally, we discuss the limitations of our current work and our plans for further studies.

4.1 Pre-training versus Training From Scratch

We explore whether pre-training strategies and tasks that are utilized in the general domain contribute to our joint representation learning in the biomedical domain. As a comparative study, we do not load the pre-trained weights and randomly initialize the weights for VisualBERT, LXMERT, and UNITER. These 3 V+L models are directly trained to classify thoracic findings without any pre-training. We train these models for 12 epochs. The results of training from scratch are shown in the *FS* columns of Table 2 and are compared to the *Default* columns. The pre-training procedure improves the averaged AUC of VisualBERT by 3%, UNITER by 2.3% and LXMERT by 2%. This confirms that the pre-training tasks contribute to generating more meaningful joint embedding. In the contrast, PixelBERT achieves state-of-the-art results in many NLP tasks in general domain, our train-from-scratch PixelBERT underperforms the other 3 pre-trained model significantly. This also indicates that pre-training is of great importance to multimodal representation learning.

4.2 BERT versus ClinicalBERT

We observe that ClinicalBERT outperforms BERT by 5.8% in MIMIC-CXR and 1.1% in OpenI. It is as expected in that ClinicalBERT is pre-trained using MIMIC-III which is also released by PhysioNet. Compared with BERT, ClinicalBERT adapts better to biomedical data. Inspired by this, we replace the BERT vocabulary and embedding layer in VisualBERT, LXMERT and UNITER by clinicalBERT. In terms of implementation, we load all the pre-trained parameters except the text embedding layer to those 3 V+L models. We also train the models for 12 epochs in hope of more training epochs will help V+L models adapt to the new vocabulary and embedding layer. The results of using ClinicalBERT components are shown in the *CB* columns of Table 3. Compared with the default configuration, we do not observe any performance boosting. We believe the 12 training epochs are still not sufficient to adjust the parameters to adapt the a new language representation model.

4.3 Trainable Visual Backbone versus Frozen Visual Backbone

We are also interested in whether a trainable visual CNN backbone is beneficial. This experiment is also conducted in the original work of PixelBERT. We adopt another configuration of PixelBERT by freezing all the layers of CheXNet, the visual backbone CNN. All other hyper-parameters and technical details remain the same. The results of the PixelBERT with a frozen CNN backbone can be found in the *NT* column of Table 3. PixelBERT with frozen CheXNet only yields a moderate averaged AUC of less than 0.8, which underperforms the default configuration of more than 15%. This indicates that it is very important to adjust the weights of the visual backbone model when applying feature map of the CNN model to generate image representations.

4.4 Visualization

Similar to [47], we first visualize selected attention maps of the best performed VisualBERT to illustrate the attention mechanism. In a), b) and c) of Fig. 2, we observe several interesting patterns. Fig. 2a shows a block pattern. Only intra-modality (text self-attention and image self-attention) can be observed in this attention map. Fig. 2b has a vertical pattern that illustrates Text-to-Image and Text-to-Text attentions in this layer. Besides, we can see some special tokens are heavily attended. Fig. 2c visualizes the attention scores of a head in the penultimate layer. Text-to-Image, Image-to-Text and Text self-attention can be found in this attention map. When comparing the difference of these 3 attention maps, we observe there is a trending that the deeper layers demonstrate more interaction between image and text, while self-attention predominate in the beginning several layers. Furthermore, to quantitatively analyze the [CLS] attention trace, we calculate the layer-level *Modality Importance (MI) scores* introduced in [48] of textual and visual

modality, respectively. The result is shown in Table 4. We can see that layer-level MI scores for text modality are significantly higher than those for visual modality, especially at intermediate layers. This suggests that more attention heads learn useful knowledge from the textual modality than image modality.

4.5 Error Analysis

For error analysis analysis, the top 10 tokens across all heads and layers with highest attention scores attended by the [CLS] token are highlighted in the Fig. 3. All three cases are sampled from OpenI. In Fig. 3a, a sample diagnosed with *Atelectasis, Pleural Effusion* is correctly classified. We can observe that keywords, such as *atelectatic collapse, opacity, effusion*, display high attention by the classification token. Visual token #9, which precisely targets the contour of the collapse of the right middle lobe, also greatly contributes to the classification. On the contrary, Fig. 3b illustrates a false negative sample. This sample is wrongly classified to positive *Pneumothorax* by our model. As shown in the radiology report of this sample, there is a large *hydropneumothorax* within the left lung. Given that all V+L models use WordPiece, which is a subword algorithm, *hydropneumothorax* is tokenized to a superset of *pneumothorax*. The tokenization mechanism of V+L models results in this kind of false positive classification. Fig. 3c demonstrates a false negative sample. This patient is diagnosed with *Cardiomegaly, Edema, and Pleural Effusion*. However, only *Edema* is identified by our classifier. When digging into the specific tokens, no finding-related words but *nodular opacity* receive a high attention score. *Pleural Effusion* in the context is truncated as we set the maximum text sequence to 128. While, we can see that visual token #8 precisely targets thoracic-spine and *T-spine* in radiology report also has a high attention score. This demonstrates the strong image-text alignment ability of V+L models.

4.6 Limitation and Future Work

Our study has several limitations, each of which brings a great opportunity for future work. First, we barely tune the hyper-parameters or CNN backbone architectures of the V+L models, which has the potential of achieving better performance. For example, we could apply deeper CNN backbones, such as ResNet152 to extract visual features for PixelBERT. Additionally, due to the limitation of computation resources, we are unable to implement domain-specific pre-training. According to the previous studies [12, 13], domain-specific pre-training will enhance the model’s adaptability and therefore improve the performance of domain-specific tasks. Finally, we only apply the pre-trained V+L models to chest X-ray datasets. We are planning to examine these models on a wider range of biomedical V+L datasets and tasks, such as BCIDR [15], VQA-Med [21] with more configurations as our next step.

5 Conclusion

In this study, we examine the ability of four transformer-based V+L models in learning joint image-text embedding from chest X-ray images and associated reports. The extrinsic evaluation shows that pre-trained V+L models outperform traditional CNN-RNN methods. Ablation studies demonstrate the advantage of joint embedding over text embedding and the benefits of the pre-training procedures. Future studies will focus on pre-training V+L models using biomedical dataset and down-stream the pre-trained models to more biomedical V+L tasks.

6 Acknowledgment

This study is supported in part by NIH grant 1R01LM013337.

References

- [1] Dongfei Yu, Jianlong Fu, Tao Mei, and Yong Rui. Multi-level attention networks for visual question answering. In *Proceedings of the IEEE Conference on Computer Vision and Pattern Recognition*, pages 4709–4717, 2017.
- [2] Jyoti Aneja, Aditya Deshpande, and Alexander G Schwing. Convolutional image captioning. In *Proceedings of the IEEE conference on computer vision and pattern recognition*, pages 5561–5570, 2018.
- [3] Kuang-Huei Lee, Xi Chen, Gang Hua, Houdong Hu, and Xiaodong He. Stacked cross attention for image-text matching. In *Proceedings of the European Conference on Computer Vision (ECCV)*, pages 201–216, 2018.
- [4] Ethan Perez, Florian Strub, Harm De Vries, Vincent Dumoulin, and Aaron Courville. Film: Visual reasoning with a general conditioning layer. In *Thirty-Second AAAI Conference on Artificial Intelligence*, 2018.
- [5] Anna Rohrbach, Marcus Rohrbach, Ronghang Hu, Trevor Darrell, and Bernt Schiele. Grounding of textual phrases in images by reconstruction. In *European Conference on Computer Vision*, pages 817–834. Springer, 2016.

- [6] Stanislaw Antol, Aishwarya Agrawal, Jiasen Lu, Margaret Mitchell, Dhruv Batra, C Lawrence Zitnick, and Devi Parikh. Vqa: Visual question answering. In *Proceedings of the IEEE international conference on computer vision*, pages 2425–2433, 2015.
- [7] Andrej Karpathy and Li Fei-Fei. Deep visual-semantic alignments for generating image descriptions. In *Proceedings of the IEEE conference on computer vision and pattern recognition*, pages 3128–3137, 2015.
- [8] Jacob Devlin, Ming-Wei Chang, Kenton Lee, and Kristina Toutanova. BERT: pre-training of deep bidirectional transformers for language understanding. *CoRR*, abs/1810.04805, 2018.
- [9] Zhilin Yang, Zihang Dai, Yiming Yang, Jaime G. Carbonell, Ruslan Salakhutdinov, and Quoc V. Le. Xlnet: Generalized autoregressive pretraining for language understanding. *CoRR*, abs/1906.08237, 2019.
- [10] Ashish Vaswani, Noam Shazeer, Niki Parmar, Jakob Uszkoreit, Llion Jones, Aidan N. Gomez, Lukasz Kaiser, and Illia Polosukhin. Attention is all you need. *CoRR*, abs/1706.03762, 2017.
- [11] Yen-Chun Chen, Linjie Li, Licheng Yu, Ahmed El Kholy, Faisal Ahmed, Zhe Gan, Yu Cheng, and Jingjing Liu. Uniter: Learning universal image-text representations. *arXiv preprint arXiv:1909.11740*, 2019.
- [12] Liunian Harold Li, Mark Yatskar, Da Yin, Cho-Jui Hsieh, and Kai-Wei Chang. Visualbert: A simple and performant baseline for vision and language. *arXiv preprint arXiv:1908.03557*, 2019.
- [13] Hao Tan and Mohit Bansal. Lxmert: Learning cross-modality encoder representations from transformers. *arXiv preprint arXiv:1908.07490*, 2019.
- [14] Jiasen Lu, Dhruv Batra, Devi Parikh, and Stefan Lee. Vilbert: Pretraining task-agnostic visiolinguistic representations for vision-and-language tasks. In *Advances in Neural Information Processing Systems*, pages 13–23, 2019.
- [15] Zizhao Zhang, Pingjun Chen, Manish Sapkota, and Lin Yang. Tandemnet: Distilling knowledge from medical images using diagnostic reports as optional semantic references. In *International Conference on Medical Image Computing and Computer-Assisted Intervention*, pages 320–328. Springer, 2017.
- [16] Jason J Lau, Soumya Gayen, Asma Ben Abacha, and Dina Demner-Fushman. A dataset of clinically generated visual questions and answers about radiology images. *Scientific data*, 5(1):1–10, 2018.
- [17] Akira Fukui, Dong Huk Park, Daylen Yang, Anna Rohrbach, Trevor Darrell, and Marcus Rohrbach. Multimodal compact bilinear pooling for visual question answering and visual grounding. *arXiv preprint arXiv:1606.01847*, 2016.
- [18] Zichao Yang, Xiaodong He, Jianfeng Gao, Li Deng, and Alex Smola. Stacked attention networks for image question answering. In *Proceedings of the IEEE conference on computer vision and pattern recognition*, pages 21–29, 2016.
- [19] Xiangwen Liu, Joe Meehan, Weida Tong, Leihong Wu, Xiaowei Xu, and Joshua Xu. Dli-it: a deep learning approach to drug label identification through image and text embedding. *BMC Medical Informatics and Decision Making*, 20:1–9, 2020.
- [20] Xin Yan, Lin Li, Chulin Xie, Jun Xiao, and Lin Gu. Zhejiang university at imageclef 2019 visual question answering in the medical domain. In *CLEF (Working Notes)*, 2019.
- [21] Asma Ben Abacha, Sadid A Hasan, Vivek V Datla, Joey Liu, Dina Demner-Fushman, and Henning Müller. Vqa-med: Overview of the medical visual question answering task at imageclef 2019. In *CLEF (Working Notes)*, 2019.
- [22] Xiaosong Wang, Yifan Peng, Le Lu, Zhiyong Lu, and Ronald M Summers. Tienet: Text-image embedding network for common thorax disease classification and reporting in chest x-rays. In *Proceedings of the IEEE conference on computer vision and pattern recognition*, pages 9049–9058, 2018.
- [23] Xiaosong Wang, Yifan Peng, Le Lu, Zhiyong Lu, Mohammadhadi Bagheri, and Ronald M Summers. Chestx-ray8: Hospital-scale chest x-ray database and benchmarks on weakly-supervised classification and localization of common thorax diseases. In *Proceedings of the IEEE conference on computer vision and pattern recognition*, pages 2097–2106, 2017.
- [24] Zizhao Zhang, Pingjun Chen, Xiaoshuang Shi, and Lin Yang. Text-guided neural network training for image recognition in natural scenes and medicine. *IEEE Transactions on Pattern Analysis and Machine Intelligence*, 2019.
- [25] Dina Demner-Fushman, Sameer Antani, Matthew Simpson, and George R Thoma. Design and development of a multimodal biomedical information retrieval system. *Journal of Computing Science and Engineering*, 6(2):168–177, 2012.

- [26] Tzu-Ming Harry Hsu, Wei-Hung Weng, Willie Boag, Matthew McDermott, and Peter Szolovits. Unsupervised multimodal representation learning across medical images and reports. *arXiv preprint arXiv:1811.08615*, 2018.
- [27] Alistair EW Johnson, Tom J Pollard, Nathaniel R Greenbaum, Matthew P Lungren, Chih-ying Deng, Yifan Peng, Zhiyong Lu, Roger G Mark, Seth J Berkowitz, and Steven Horng. Mimic-cxr-jpg, a large publicly available database of labeled chest radiographs. *arXiv preprint arXiv:1901.07042*, 2019.
- [28] Jeremy Irvin, Pranav Rajpurkar, Michael Ko, Yifan Yu, Silvana Ciurea-Ilcus, Chris Chute, Henrik Marklund, Behzad Haghgoo, Robyn Ball, Katie Shpanskaya, et al. Chexpert: A large chest radiograph dataset with uncertainty labels and expert comparison. In *Proceedings of the AAAI Conference on Artificial Intelligence*, volume 33, pages 590–597, 2019.
- [29] Yifan Peng, Xiaosong Wang, Le Lu, Mohammadhadi Bagheri, Ronald Summers, and Zhiyong Lu. Negbio: a high-performance tool for negation and uncertainty detection in radiology reports. *AMIA Summits on Translational Science Proceedings*, 2018:188, 2018.
- [30] Dina Demner-Fushman, Marc D Kohli, Marc B Rosenman, Sonya E Shooshan, Laritza Rodriguez, Sameer Antani, George R Thoma, and Clement J McDonald. Preparing a collection of radiology examinations for distribution and retrieval. *Journal of the American Medical Informatics Association*, 23(2):304–310, 2016.
- [31] Carolyn E Lipscomb. Medical subject headings (mesh). *Bulletin of the Medical Library Association*, 88(3):265, 2000.
- [32] Tsung-Yi Lin, Michael Maire, Serge Belongie, James Hays, Pietro Perona, Deva Ramanan, Piotr Dollár, and C Lawrence Zitnick. Microsoft coco: Common objects in context. In *European conference on computer vision*, pages 740–755. Springer, 2014.
- [33] Ranjay Krishna, Yuke Zhu, Oliver Groth, Justin Johnson, Kenji Hata, Joshua Kravitz, Stephanie Chen, Yannis Kalantidis, Li-Jia Li, David A Shamma, et al. Visual genome: Connecting language and vision using crowdsourced dense image annotations. *International journal of computer vision*, 123(1):32–73, 2017.
- [34] Piyush Sharma, Nan Ding, Sebastian Goodman, and Radu Soricut. Conceptual captions: A cleaned, hypernymed, image alt-text dataset for automatic image captioning. In *Proceedings of the 56th Annual Meeting of the Association for Computational Linguistics (Volume 1: Long Papers)*, pages 2556–2565, 2018.
- [35] Yuke Zhu, Oliver Groth, Michael Bernstein, and Li Fei-Fei. Visual7w: Grounded question answering in images. In *Proceedings of the IEEE conference on computer vision and pattern recognition*, pages 4995–5004, 2016.
- [36] Peter Anderson, Xiaodong He, Chris Buehler, Damien Teney, Mark Johnson, Stephen Gould, and Lei Zhang. Bottom-up and top-down attention for image captioning and visual question answering. In *Proceedings of the IEEE conference on computer vision and pattern recognition*, pages 6077–6086, 2018.
- [37] Drew A Hudson and Christopher D Manning. Gqa: a new dataset for compositional question answering over real-world images. *arXiv preprint arXiv:1902.09506*, 3(8), 2019.
- [38] Vicente Ordonez, Girish Kulkarni, and Tamara L Berg. Im2text: Describing images using 1 million captioned photographs. In *Advances in neural information processing systems*, pages 1143–1151, 2011.
- [39] Zhicheng Huang, Zhaoyang Zeng, Bei Liu, Dongmei Fu, and Jianlong Fu. Pixel-bert: Aligning image pixels with text by deep multi-modal transformers, 2020.
- [40] Saining Xie, Ross B. Girshick, Piotr Dollár, Zhuowen Tu, and Kaiming He. Aggregated residual transformations for deep neural networks. *CoRR*, abs/1611.05431, 2016.
- [41] Jacob Devlin, Ming-Wei Chang, Kenton Lee, and Kristina Toutanova. Bert: Pre-training of deep bidirectional transformers for language understanding. *arXiv preprint arXiv:1810.04805*, 2018.
- [42] Yukun Zhu, Ryan Kiros, Rich Zemel, Ruslan Salakhutdinov, Raquel Urtasun, Antonio Torralba, and Sanja Fidler. Aligning books and movies: Towards story-like visual explanations by watching movies and reading books. In *Proceedings of the IEEE international conference on computer vision*, pages 19–27, 2015.
- [43] Emily Alsentzer, John R Murphy, Willie Boag, Wei-Hung Weng, Di Jin, Tristan Naumann, and Matthew McDermott. Publicly available clinical bert embeddings. *arXiv preprint arXiv:1904.03323*, 2019.
- [44] Alistair EW Johnson, Tom J Pollard, Lu Shen, H Lehman Li-Wei, Mengling Feng, Mohammad Ghassemi, Benjamin Moody, Peter Szolovits, Leo Anthony Celi, and Roger G Mark. Mimic-iii, a freely accessible critical care database. *Scientific data*, 3(1):1–9, 2016.
- [45] Alexey Romanov and Chaitanya Shivade. Lessons from natural language inference in the clinical domain. *arXiv preprint arXiv:1808.06752*, 2018.

- [46] Pranav Rajpurkar, Jeremy Irvin, Kaylie Zhu, Brandon Yang, Hershel Mehta, Tony Duan, Daisy Yi Ding, Aarti Bagul, Curtis Langlotz, Katie S. Shpanskaya, Matthew P. Lungren, and Andrew Y. Ng. Chexnet: Radiologist-level pneumonia detection on chest x-rays with deep learning. *CoRR*, abs/1711.05225, 2017.
- [47] Olga Kovaleva, Alexey Romanov, Anna Rogers, and Anna Rumshisky. Revealing the dark secrets of bert. *arXiv preprint arXiv:1908.08593*, 2019.
- [48] Jize Cao, Zhe Gan, Yu Cheng, Licheng Yu, Yen-Chun Chen, and Jingjing Liu. Behind the scene: Revealing the secrets of pre-trained vision-and-language models. *arXiv preprint arXiv:2005.07310*, 2020.